A Predictive Tool for Determining the Patient-Specific Mechanical Properties of the Human Corneal Tissue

Miguel Ángel Ariza–Gracia[a,b], Santiago Redondo[a], David Piñero Llorens[c,d], Begoña Calvo[a,f], José Felix Rodriguez Matas[e]

[a]*Department of Mechanical Engineering, Aragón Institute of Engineering Research –i3A–, Zaragoza, Spain*
[b]*Institute for Surgical Technology and Biomechanics, University of Bern, Switzerland*
[c]*Ophthalmology Department –OFTALMAR–, Medimar International Hospital, Alicante, Spain*
[d]*Optics, Pharmacologist and Anatomy Department, University of Alicante, Alicante, Spain*
[e]*LaBS, Department of Chemistry, Materials and Chemical Engineering "Giulio Natta", Politecnico di Milano, Milano, Italy*
[f]*CIBER de Bioingeniería, Biomateriales y Nanomedicina (CIBER-BBN), Aragon Health Sciences Institute, Spain*

Abstract

A computational predictive tool for assessing the patient specific corneal tissue properties is developed. The predictive tool considers as input variables the corneal central thickness (CCT), the intraocular pressure (IOP), and the maximum deformation amplitude of the corneal apex (U) when subjected to a Non–Contact Tonometry test. The proposed methodology consists on two main steps. First, an extensive dataset is generated by means of Monte Carlo (MC) simulations based on finite element models with patient specific geometric features that simulates the non-contact tonometry test. The cornea is assumed to be an anisotropic tissue in order to reproduce the mechanical behavior observed experimentally. A clinical database of 130 patients (53 healthy, 63 keratoconic and 14 post-LASIK surgery) is used for generating a dataset of more than 9,000 cases, by permuting the material properties. The second step consist on building predictive models for the material parameters of the constitutive model as a function of the input variables. Four different approximations are explored: Quadratic Response Surface (QRS) approximation, Multiple Layer Perceptron (MLP), Support Vector Regressor (SVR), and K-nn search. The models were validated against data from five real patients. The material properties obtained with the predicted models lead to a simulated corneal displacement within a 10% error of the measured value on the worst case scenario of a patient with a very advanced keratoconus disease. These results demonstrate the potential and soundness of the proposed methodology.

Keywords: Corneal Biomechanics, Finite Element modeling, Monte Carlo Analysis, Patient-Specific Material

1. Introduction

Corneal Biomechanics is an open topic in ophthalmology. A precise knowledge about the underlying factors affecting the corneal mechanical response will allow establishing better clinical diagnoses, monitoring the progression of different diseases (e.g. the Keratoconus, a non-inflammatory disease causing the disruption of the collagen fibers) or designing a priori patient-specific surgical plans that may reduce the occurrence of unexpected outcomes.

Recently, non–contact tonometry has gained interest as a diagnosis tool in ophthalmology, and as an alternative way of characterizing the mechanical behavior of the cornea. In a non-contact tonometry test, a high-velocity air jet is applied on the cornea for a very short time (less than 30 ms), causing the cornea to deform, while the corneal motion is recorded by a high speed camera. A number of biomarkers associated with the corneal motion i.e., maximum corneal displacement, time between first and second applanation, among others, have been proposed to characterize pre and post-operative biomechanical changes[1, 2, 3, 4, 5, 6, 7, 8, 9]. However, this response is the result of the interplay between the geometry of the cornea, the intraocular pressure (IOP), and the mechanical behavior of the corneal tissue, as has been demonstrated by recent experimental and numerical studies [2, 10]. These studies suggest that this interplay could be the cause of some unexpected clinical results (i.e. a softer cornea with a higher IOP could show the same behavior as a stiffer cornea with a lower IOP). Although the geometry and the IOP can be measured by means of corneal topographers and the Goldmann Tonometry Applanation tests (GAT), the mechanical behavior of the cornea cannot be directly characterized *in-vivo*.

The human cornea is composed of an almost incompressible layered ground material (matrix), mainly composed of water, where two families of orthogonal collagen fibers are embedded [11, 12]. Due to this structure, the tissue behaves as an anisotropic solid having two preferential

Email address: mariza.at.unizar.es (Miguel Ángel Ariza–Gracia)

directions in correspondence with the direction of the collagen fibers. A number of material models have been proposed to reproduce the corneal behavior, ranging from simply hyperelastic isotropic materials [13] to more complex models coupling the hyperelastic isotropic response for the matrix (Neo–Hookean models) with the anisotropic response of the collagen fibers of the eye [12, 14, 15, 16, 17, 18, 23, 24]. These material models have been incorporated into computer models of the eye to simulate surgical interventions and tonometry tests in an effort to demonstrate the potentiality of these *in-silico* models[3, 4, 17, 25, 26, 27, 28, 54, 55, 56].

Numerical studies have found, however, that the contribution of the fibers to load bearing during a tonometry test is highly reduced due to the bending mode of deformation imposed by the test. Under this particular loading, other factors such as the IOP or the central corneal thickness (CCT) were found to be more significant in the response of the cornea to the air-puff[2, 4]. Moreover, in the physiological range of IOP (from 10 to 15 mmHg) and CCT (from 500 to 600 microns), the corneal tissue is not subjected to large stresses, with the fibers bearing relatively low load[4]. In addition, experimental studies in porcine and human eyes demonstrate that fibers play a major role when the IOP increases to values above the physiological range and not otherwise [24, 29]. Therefore, it seems that the mechanical behavior of the matrix will play a significant role in reproducing the corneal response during a tonometry test. Furthermore, some authors have suggested that only one in-vivo technique could not be accurate enough for characterising the material properties properly Kok et al. [19, 4]. However, by now it is the only clinical device that allows a non-invasive analysis of the human cornea whereas biaxial or inflation tests only can be carried out ex-vivo.

In the last decade, with the advent of large and extensive datasets, the use of Artificial Neural Networks (ANN) have come back to the spotlight. Basically, an ANN intends modeling the human brain by mathematically reproducing the neural architecture to learn and recognise patterns or to adjust functional response. In ophthalmology, commercial topographers implement different types of ANN to establish a classification between healthy eyes and diseased eyes (e.g. keratoconus eyes, KTC, or ectasias post-LASIK)[30, 31, 32, 33, 34]. Unfortunately, these ANNs are mainly based on the geometrical features of the cornea (e.g. radii, thickness, diopters, shape

factors...) and is not usual to consider mechanical variables as the intraocular pressure (IOP). In addition to the ANN, the Response Surface methods have also been used in biomedical sciences for predicting the effects of different model parameters on a set of biomarkers associated with a particular pathology [35, 36, 37]. The great interest of these mathematical methods relies on the immediateness of their response, a key factor for a clinical application. However, they suffer from an important weakness: the extension of the training dataset. These methods based on learning precise of a great amount of data in different conditions that lead to a proper and accurate response of the system. Otherwise, a poor prediction or an overfitting in the solution could be reached with catastrophic results. Unfortunately, the higher the complexity of the applied neural network, the higher the number of cases needed for both, training and validating the training. Therefore, this is a clear limiting factor when dealing with patient data. Apart from the aforementioned mathematical tools, other optimization approach has been used for determining the material properties of the human cornea: the inverse finite element method (hereafter IFEM) [3, 20, 21, 22]. This method uses an iterative optimization procedure that changes a set of unknown parameters so as to match the numerical response with the experimental response. Thus, it requieres of a great accuracy on the definition of the problem and the boundary conditions to be reliable enough. Besides, each case of interest must be evaluated ad-hoc resulting on a time-consuming process which is not real-time and, hence, not interesting for real clinical application.

The present work aims to build predictors for real-time clinical application, based on ANN and Quadratic Response Surface (QRS) approximations, to obtain the parameters of the constitutive model of the patient's cornea using 3 clinical biomarkers: the maximum corneal displacement measured during a non–contact tonometry test (U), the patient's IOP, and geometrical features of the cornea as inputs. The predictive tool relies on a dataset generated by the results of finite element simulations of the non-contact tonometry test. The simulations are based on combinations of patients of the real clinical database (the patient-specific corneal geometry and the Goldmann IOP[4]) and of corneal material properties of the numerical model so as to predict the corneal apical displacement. In brief, the finite element model is used to perform a Monte Carlo (MC)

simulation in which the material parameters, and the IOP are uniformly varied within an established range. The range for the material parameters was determined by considering experimental results from inflation test reported in the literature[24, 38] and the physiological response of the cornea to an air-puff device (i.e. displacement of the cornea using a CorVis device). First, the inflation tests are used for initially screening the model parameters, for constraining the space of search of the optimization and trying to avoid an ill-posed solution [19]. Second, the range of each material parameter was then determined such that the *in-silico* inflation curve was within the experimental window. In this vein, both physiological behaviours of the cornea are fulfilled at the same time: the response to an inflation test (biaxial stress) and the response to an air-puff test (bending stress). Afterwards, the generated dataset is then used to implement different predictors for the mechanical properties of the patient's corneal model in terms of variables that are identified in an standard non-contact tonometry test. Eventually, the resulting models are tested on five different, new and unknown patients to show the potential and soundness of the proposed methodology on behalf of the prediction of the corneal tissue properties.

2. Material and Methods

2.1. Patients data

Topographical data of the cornea and IOP from 130 patients (53 healthy, 63 keratoconic and 14 post-LASIK surgery)[2, 4] was collected prospectively, i.e. an ongoing measuring process without posterior revision of the patient's medical history, at the Department of Ophthalmology (OFTALMAR) of the Vithas Medimar International Hospital (Alicante, Spain). A comprehensive ophthalmologic examination was performed in all cases including: Goldmann tonometry and analysis of the corneal anterior and posterior segments by means of a Scheimpflug photography-based topography system (Pentacam system, Oculus, Germany). Inclusion criteria were: healthy eyes, eyes with the diagnosis of keratoconus according to the Rabinowitz criteria [39], and eyes that had undergone previous laser in situ keratomileusis (post-LASIK) for the correction of myopia (range, -0.50 to -8.00 D). Exclusion criteria were patients with active ocular diseases or patients with other types of previous ocular surgeries. Clinical validation data was collected

prospectively at the Qvision Ophthalmic Unit of the Vithas Virgen del Mar Hospital (Almeria, Spain). A comprehensive ophthalmologic examination was performed in all cases including: Goldmann tonometry, corneal and anterior segment analysis by means of a Scheimpflug photography-based topography system (Pentacam, Oculus, Germany) and the corneal dynamics analysis (CorVis, Oculus, Germany). The study adhered to the tenets of the Declaration of Helsinki and was approved by the ethics committee of the University of Alicante (Alicante, Spain).

Figure 1: **Graphic Outline of the Developed Methodology.**

2.2. Construction of the predictive model

Figure 1 shows the main steps of the proposed methodology. As stated in the introduction, the methodology relies on the use of a previously developed algorithm for the patient–specific geometrical reconstruction of the cornea and the simulation of a non–contact tonometry test [4]. For generating the dataset, two main steps have to be differentiated. In a first step, an initial screening over the constitutive model parameters is performed using the inflation experiments reported in the literature [24, 38]. There is a double benefit on doing it: constraining the space of solutions for the subsequent step and restraining the space of solutions to those that behaves physiologically on the inflation range. The second step corresponds to the generation of the training dataset using a Monte Carlo analysis. The *in-silico* simulations of the non-contact tonometry test using the clinical patient-specific corneal topography and the clinical Goldmann IOP are used to obtain the bending behaviour of the cornea. Filtering with the clinical ranges of maximum deformation amplitude [1], the space of material parameters that behaves physiologically in both experiments (inflation and air-puff) is obtained. Following the Monte Carlo simulation, an Analysis of Variance (ANOVA, using a second order linear model for the sum of the squares and accounting for interaction between the parameters) is performed to identify the impact of the variables on the maximum displacement of the corneal apex, so defining the main inputs of the predictors. The resulting dataset is then used to train a set of 4 different predictors in terms of the material model

parameters (D_1, D_2, k_1, k_2) and the main variables identified with the ANOVA. Finally, the predictors are tested with clinical results from a non-contact tonometry test on five patients so as to validate the methodology using unknown patient data.

2.3. Finite Element Model

The FE model comprises the patient–specific corneal geometric data where it is provided by the topographer, the limbus and half of the sclera [4]. The geometry is meshed using quadratic hexahedral elements (62,276 nodes and 13,425 elements). The limbus and the cornea are considered as anisotropic solids described by the same strain energy function but with different preferential directions (the cornea is assumed as orthotropic with two orthogonal families of fibers, whereas the limbus is assumed to be transversely isotropic with only one family of fibers). The limbus is assumed to have the same material properties as the cornea since a proper in-vivo characterization has not been reported yet, and as it is considered as a mere more compliant boundary condition for the cornea [56] far from the zone of influence of the air-jet. Material models are described in detailed in the following section. On the contrary, the sclera is assumed as an isotropic solid since the region of interest is far from the optic nerve insertion. Symmetry boundary conditions are defined on the scleral symmetry plane and the intraocular pressure is assumed as an internal pressure equally distributed determined by the Goldmann tonometry test.

To properly simulate the profile of pressure over the cornea of the non–contact tonometry from a pure structural point of view, a computer fluid dynamics simulation using ANSYS was carried out to determine the pressure pattern over the cornea due to the air-puff. Although it is an approximation since the cornea is considered as a rigid wall interface for the sake of the fluid analysis, a bell-shaped profile with a peak pressure set to 15 kPa is obtained (commercial devices range between 10 and 15 kPa), following a 30 ms temporal load profile provided by Oculus (only the load phase is considered). In addition, a zero–pressure algorithm is performed as a previous step to the air-puff simulation and necessary for determining the corneal tissue pre-stress due to the IOP. Briefly, a fixed-point iterative optimization is applied where an initial model of the eyeball is subjected to an internal pressure to deform. Subsequently, the error between the measured configuration (i.e. topographer geometry) and the deformed configuration is computed.

If the error is greater than a tolerance, a new initial model is computed by subtracting the point-to-point error. Eventually, the algorithm stops once the measured reference is achieved when pressurising the initial (usually smaller) model (see further information in [4])

2.4. Material Model

The form of the strain energy function for modeling the cornea corresponds to a modified version of that proposed by Gasser–Holzapfel–Ogden [40] for arterial tissue, where the neo-hookean term has been substituted by an exponential term

$$\psi(C, n_\alpha) = D_1 \cdot \{\exp[D_2 \cdot (\bar{I}_1 - 3)] - 1\} + \frac{k_1}{2 \cdot k_2} \cdot \sum_{\alpha=1}^{N} \{\exp[k_2 \langle \bar{E}_\alpha \rangle^2] - 1\} + K_0 \cdot \left(\frac{J_{el}^2 - 1}{2} - \ln(J_{el}) \right),$$
$$\text{with } \bar{E}_\alpha \overset{\text{def}}{=} \kappa \cdot (\bar{I}_1 - 3) + (1 - 3\kappa) \cdot (\bar{I}_{4(\alpha\alpha)} - 1), \tag{1}$$

where C is the right Cauchy–Green tensor, $J_{el} = \sqrt{\det C}$ is the elastic volume ratio; D_1, D_2, k_1 and k_2 are material parameters, and K_0 is the bulk modulus; N is the number of families of fibers; $\bar{I}_1$ is the first invariant of the modified right Cauchy–Green Tensor $\bar{C} = J_{el}^{-2/3} C$, and $\bar{I}_{4(\alpha\alpha)} = n_\alpha \cdot \bar{C} \cdot n_\alpha$ is the square of the stretch along the fiber's direction n_α. The parameter κ describes the level of dispersion in the fibers direction, and has been assumed to be zero, since it has been reported that a dispersion in the fibers of ± 10 deg about the main direction results on a maximum variation of a 0.03% on the maximum corneal displacement [4].

The strain like term, $\bar{E}_\alpha$ in Eq. 1 characterizes the deformation of the family of fibers with preferred direction n_α. The model assumes that collagen fibers bear load only in tension while buckle under compressive loading. Hence, only when the strain of the fibers is positive, i.e., $\bar{E}_\alpha > 0$, the fibers contribute in the strain energy function. This condition is enforced by the term $< \bar{E}_\alpha >$, where the operator $< \cdot >$ stands for the Macauley bracket defined as $< x >= \frac{1}{2}(|x| + x)$. The model has been implemented in a *UANISOHYPER* user subroutine within the FE software *Abaqus*.

Due to the random distribution of fibers far from the optical nerve insertion, the sclera has

been assumed as an isotropic hyperelastic material [41] (Eq. 2).

$$\psi_Y = \sum_{i=1}^{3} K_i (J_{el} - 1)^{2 \cdot i} + \sum_{i=1}^{3} C_{i0} \cdot (\bar{I}_1 - 3)^i, \tag{2}$$

with $C_{10} = 810$ [kPa], $C_{20} = 56,050$ [kPa], $C_{30} = 2,332,260$ [kPa], K_i [kPa] is automatically set by the finite element solver during execution.

2.5. Monte Carlo Simulation

Due to the large dispersion in the corneal responses to inflation and air-puff tests and to the fact that the behaviour of the fibers should not be properly characterized by a single experiment, the Monte Carlo simulation was conducted in two steps. First, the inflation experiments were used for screening on the range of values of the material model that behaves physiologically in a biaxial stress state and, hence, constraining the searching space in subsequent steps. A total of 81 combinations of the material parameters were used to simulate an inflation test on an average healthy eye (see Figure 2b). The *in-silico* inflation curves were then compared with experiments reported in the literature [24, 38] and the range of material parameters leading to curves within the experimental window was determined. The identified range of parameters was set to: $D_1[kPa] \in (0.0492, 0.492)$, $D_2[-] \in (70, 144)$, $k_1[kPa] \in (15, 130)$, and $k_2[-] \in (10, 1000)$.

The second step is to generate the dataset using the Monte Carlo simulation and considering a uniformly distributed samples of the material parameters within the previously identified range. A uniform distribution is assumed since there are no a priori data on the dispersion of the mechanical parameters in human cornea and, therefore, a total ignorance about the population is assumed. Otherwise, a bias could be introduced on the outcome of the system. Additionally and to account for the physiological diurnal variations in the IOP [42], variations in the IOP ranging from 8 to 30 mmHg along with the patient's IOP at the moment of the examination, were also considered in the Monte Carlo simulation. Hence, for each available geometry in the clinical database, 72 different samples of the material parameters and the IOP, uniformly distributed in their respective ranges, were used to conducted 72 simulations of the non-contact tonometry test. As a result, a total of 9,360 computations (i.e. 72 combinations times 130 geometries) were

scheduled. The generated dataset comprised the following variables: Classification (Healthy, KTC and LASIK), Computation Exit Status (Failed or Successful), Material Parameters (D_1, D_2, k_1 and k_2), IOP, CCT, Nasal–Temporal Curvature (R_h), Superior–Inferior Curvature (R_v) and the computed maximum displacement of the cornea (U_{num}).

Once the dataset was generated, an ANOVA analysis was performed to identify the most influential model parameters (geometry, pressure and material) on the numerical displacement, U_{num}, obtained with the non–contact tonometry simulation. Results from this analysis were used to identify the geometric parameters to be include in the construction of the predictor functions for the material parameters. The ANOVA was conducted on the global dataset without differentiation between the populations, and for each of the populations (Healthy, Keratoconus or KTC, and LASIK). Since the dataset is randomly generated, an ANOVA analysis cannot be directly conducted on the data. Instead, a Quadratic Response surface is first fitted to U_{num} (e.g., $U_{num} = f(geometry, pressure, material)$). Then, a Pareto analysis (i.e. it states the most influential parameters on an objective variable, arranging them in decreasing order by taking into account the cumulative sum of the influence until reaching a 95% of the variation on the objective variable) is used to determine the most influential parameters on the dependent variable, U_{num}.

2.6. Predictive Models

The generated dataset is used to build predictors for the mechanical properties of the patient's cornea in terms of variables that are measured with an standard non-contact tonometry test. Two different approaches are implemented (see in Fig.1): i) Response surface approach, and ii) Neighborhood–Based approach.

2.6.1. Response surface approach

This approach is based on adjusting, or training, a predictor model for each material parameter (D_1, D_2, k_1 and k_2). Individual predictors are build using either ANN or a quadratic response surface. For the ANN approach, two different mathematical models were considered, namely: Multiple Layer Perceptron, MLP, and Support Vector Regressor, SVR. Alternatively to the ANN, a quadratic RS (QRS) was fitted for each material parameter.

Artificial Neural Network: Multiple Layer Perceptron (MLP). An MLP is a feedforward ANN whose aim is mapping a set of input variables (i.e. parameters that define the problem) into an output, allowing to distinguish non-linear separable sets. It consists of different layers formed by 'neurones' or processing elements with non-linear activation: input layer, hidden layer and output layer. This technique a supervised back-propagation learning technique for the training [57]. For the present study, an ensemble of 7 independent MLP has been configured, obtaining the output as the average of the individual outputs (reducing the inherent variability of the method). Each independent MLP has been trained using a Levenberg–Marquardt minimisation with early stooping criteria (usual criteria: a maximum of 6 increments of the validation error and a maximum of 1000 training epochs). Each MLP has 10 neurones for the hidden layer.

Support Vector Regressor (SVR). A Support Vector Machine (SVM) is a supervised learning model that is mainly use for analyse data for classification and regression analysis [58]. Once a set of training is given, it marks each point for classifying into categories using a non-probabilistic non-linear classifier based on the use of kernels, which allow the mapping into higher-dimensional feature spaces so as to better discern the clustering of categories. When the SVM is used for fitting a response (i.e. regression) instead of classifying, it is called a Support Vector Regressor (SVR)[59]. For the present study, the libSVM C++ library using the epsilon–SVR formulation with a gaussian kernel (RBF) was used for solving the SVR problem [43]. The configuration parameters are three: the *epsilon value* (default value 0.001), the algorithm *Cost* (value optimised) and the kernel's *Gamma* (value optimised). The optimisation of the parameters were achieved by searching the *cross-validation generalised performance* of the training data. This method uses a grid search within a the maximum expectation range of the parameters (*Cost* and *Gamma*) yielding a surface were the minimum corresponds to the optimum.

Concerning the dataset used for both methods (MLP and SVR), it has been split on an 80% of data for the training stage and a 20% for the validation stage. Besides, the models have been trained using k-fold techniques (with a k-fold equals to 5), to automatically optimise

their parameters while avoiding the overfitting during the training and differencing datasets according to populations (Healthy, KTC and LASIK). In addition, the data has been normalised using the criterion of null average and the standard deviation equal to one.

Quadratic Response Surface (QRS). The response surface methodology seeks for the relationship between the input variables and the response variables in terms of the optimal response and using a dataset built following a sequence of designed experiments [60]. Generally speaking, the method fits a multiple order surface (e.g. a second order polynomial) so as to minimize the error with respect to the experimental data. For the present study, a multiple linear regression model including crossed and second order terms was used for predicting the response (D_1, D_2, k_1 and k_2) as a linear function of predictor variables. The model fitting used a stepwise regression (i.e. terms can be added or removed depending on its influence on the response) based on the Akaike Information Criterion (AIC) [44]. The AIC provides a measure of model quality by simulating the situation where the model is tested on a different data set. After computing several different models, they can be compared using this criterion. According to Akaike's theory, the most accurate model has the smallest AIC.

Independent predictors were fitted to the entire dataset, and to individual populations in order to test their classification capabilities. Each predictor is structured as follows. Let j stands for a particular material parameter, and χ_j its predictor. Based on the ANOVA analysis performed on the dataset, the most influential geometric parameters on the corneal displacement, U, are identified and denoted as x. Hence, each predictor χ_j is build as a function (inputs) of: x, IOP, and the remaining material parameters of the model. Therefore, for parameter D_1, $\chi_{D_1} = \chi_{D_1}(x, IOP, D_2, k_1, k_2)$.

Once the models are trained, identification of the material parameters from the known patient data i.e., x, IOP, and U, is performed iteratively using a fixed-point iteration algorithm. The search algorithm is detailed in Algorithm 1. In brief, D_1 is evaluated through χ_{D_1} using the material parameters from the previous iteration; D_2 will then be obtained through χ_{D_2} including the previously computed value for D_1 while, k_1 and k_2 are kept from the previous iteration, and

so on. The cost function controls the changes in value of the material parameters between two consecutive iterations: if the change in the material properties between two consecutive iterations is less than a tolerance, the algorithm stops and the identified material parameters are reported.

Algorithm 1. *Fixed-Point iteration algorithm to determine Material Parameters from patient's data (Clinical Biomarkers).*

%Initialise Control Values
TOL=1e-6; itemax=5000; k=1; error=1;
%Initialise Random Material Seed
mat^k=(D_1^k D_2^k k_1^k k_2^k);
WHILE *AND(error>TOL,k<itemax)*
  %Predict D_1^{k+1}
  D_1^{k+1}:=χ_{D_1}(x,IOP, U, D_2^k, k_1^k, k_2^k);
    %Predict D_2^{k+1}
    ↳D_2^{k+1}:=χ_{D_2}(x,IOP, U, D_1^{k+1} k_1^k k_2^k);
      %Predict k_1^{k+1}
      ↳k_1^{k+1}:=χ_{k_1}(x,IOP, U, D_1^{k+1}, D_2^{k+1}, k_2^k);
        %Predict k_2^{k+1}
        ↳k_2^{k+1}:=χ_{k_2}(x,IOP, U, D_1^{k+1}, D_2^{k+1}, k_1^{k+1});
  %Check Cost Function
  mat^{k+1}=(D_1^{k+1}, D_2^{k+1}, k_1^{k+1}, k_2^{k+1});
  error=$\sum |mat^{k+1} - mat^k|$;
  %Update Next Iteration
  k=k+1;
END

2.6.2. Neighborhood–Based Protocol (K–nn Search)

Due to the coupled effects that Geometry, IOP, and material properties have on Corneal Response (i.e. displacement), there could exist different combinations of parameters that give the same maximum displacement (i.e. less rigid corneas subjected to a large IOP could experience the same displacement to the air-puff as a more rigid cornea subjected to a lower IOP) causing the Response Surface approach to be less effective, i.e., Algorithm 1 could identify different sets of material parameters according to the initial seed (local minima). The K–nn Search approach searches the set of material parameters directly in the raw dataset without the need of an approximation function. The algorithm searches the n closest neighbors to the patient in the dataset and then interpolate the material model parameters in terms of the distance from the Patient's point to the neighbors. The distance is calculated as the Euclidean distance in the (x, IOP, U) subspace

of the dataset.

2.7. Validation

To validate the proposed methodology, 5 eyes (1 healthy eye and 4 keratoconus eyes) that were subjected to a non-contact tonometry test (CorVis ST, Oculus, Germany) were considered. For these eyes, the corneal topography, IOP and, corneal displacement due to the air-puff, U, were available (see Table 1). These parameters were used to predict the Patient's material model parameters using the predictors previously described. With the predicted material model parameters, and the topographical data of the cornea, an *in-silico* non-contact tonometry test is simulated using the procedure proposed in [4]. The numerical corneal displacement, U_{num}, was compared to the clinical displacement U.

Table 1: **Clinical Validation Data: CorVis Non–Contact Tonometry Test for validation patients (5 eyes: 1 healthy eye and 4 keratoconus eyes).**

L.	**Eye**	**IOP**	**CCT**	**U**	**AL1**	**AL2**	**VA1**	**VA2**	**P. Dist.**	**R**
h_0	R	12	578	1.00	2.09	1.92	0.19	-0.36	2.38	7.5
ktc_0	R	15	545	1.12	1.81	1.87	0.16	-0.34	5.07	7.58
ktc_1	L	15	544	1.03	1.84	2.06	0.18	-0.38	5.08	7.9
ktc_2	R	15	464	1.05	1.87	1.07	0.16	-0.43	2.53	7.6
ktc_3	L	16	460	1.12	1.84	2.06	0.17	-0.39	5.45	7.81

Table Legend and Units. **L.**: identification tag (i.e. 'h' for healthy eyes and 'ktc' for keratoconus eyes); **Eye**: ocular position; **IOP** [mmHg]: intraocular pressure; **CCT** [μm]: central corneal thickness; **U** [mm]: maximum deformation amplitude at the maximum concavity time; **AL1** [mm]: first applanation length ; **AL2** [mm]: second applanation length; **VA1** [mm/s]: velocity at the first applanation time; **VA2** [mm/s]: velocity at the second applanation time; **P. Dist.** [mm]: peak distance; **R** [mm]: curvature at the maximum concavity time.

2.8. Computations and Statistical analysis

Finite element simulations were conducted on the commercial finite element software Abaqus 6.11 (Dassault Systèmes Simulia Corp.) All the mathematical computations, algorithms and statistical analysis have been developed using MATLAB R2012 v.8.0. software and open source C++ libraries (libSVM C++, [43]).

Data is reported by their mean and standard deviation (mean ± SD), respectively. Statistical significance was tested with the two-sample Kolmogorov-Smirnov test, where a two-sided p-value of less than 0.05 determined significance. Performance of the predictors was measured in terms of the coefficient of correlation R^2, to measure the quality of the fitting, whereas the Akaike Information Criterion (AIC) [44] was used to directly compared the quality of each model relative to each other.

3. Results

3.1. Monte Carlo Simulation

The Monte Carlo simulation computed 9,360 combinations. Due to technical limitations regarding the number of licenses, computations were performed on two conventional PCs with 8 core processor and 8 GB RAM required 128 days of computations on double thread. However, the methodology is implemented for a suitable parallel and massive computation on a computational cluster. The failure rate was under the 3% of the computations, resulting on an effective dataset of 9,216 cases.

Figure 2: **Results of the Monte Carlo simulation. (a)** Mechanical corneal response to both experiments: inflation and air-puff. The physiological range for the inflation is limited by the inflation real curves reported in the literature [24, 38] (see in black dashed lines and triangles) whereas the physiological range of the air-puff behaviour must lay within the 'Searching Objective Frame' (i.e. the reported experimental displacement to CorVis [1]). As it can be observed in the 'upper right area', a physiological inflation behaviour could not represent a physiological air-puff mechanical response and, thus, aiming out of the searching frame (see yellow vs. red lines in figure); **(b)** First Monte Carlo analysis for pre-screening the range of the material parameters within the physiological inflation range reported. From all the simulations, the extreme ones were chosen for constraining the space of search of the second Monte Carlo analysis. The range of the material parameters is shown in the bottom of the panel; **(c)** Second Monte Carlo analysis for establishing the range of the corneal mechanical response to an air-puff test. All the mechanical responses (incremental displacement due to the incremental pressure) related to the material range variation are depicted in a lighter color in figures. Darker zones belong to those combinations of material parameters that numerically behaved as physiological with respect to the maximum deformation amplitude reported in CorVis diagnosis. **(c.1)** Results of the Monte Carlo simulation for those eyes classified as healthy on the clinic (i.e. those whose topography and IOP were diagnosed as healthy by an optometrist). Dark red curves belong to the simulations that cast a numerical displacement that is contained within the experimental range ($U_{Healthy}[mm] \in (0.8, 1.1)$); **(c.2)** Results of the Monte Carlo simulation for those eyes classified as keratoconic on the clinic. Dark blue curves belong to the simulations that cast a numerical displacement that is contained within the experimental range ($U_{KTC}[mm] \in (0.95, 1.25)$); **(c.3)** Results of the Monte Carlo simulation for those eyes that were subjected to a LASIK surgery on the clinic. Dark green curves belong to the simulations that cast a numerical displacement that is contained within the experimental range ($U_{LASIK}[mm] \in (0.9, 1.15)$).

The simulations show that the proposed material model is adequate to reproduce both, the inflation and the bending response of the cornea when subjected to an air-puff for different levels of

the IOP (see Fig.2.a). In particular, the range of parameters used for the Monte Carlo simulation is able to accommodate the experimental response to corneal inflation tests reported in the literature (see Fig. 2.b). Note that, traditional model development for corneal mechanics has mainly considered inflation tests to identify the model parameters. However, when the response to an air-puff is considered, we found that there are a number of combinations for which the inflation response is within the experimental range but the corneal displacement due to the air-puff is not. An example of this situation is given by the red and blue lines in Fig. 2.a. In both cases the response to the inflation test is identical, but the response to the air-puff is not physiological for the red line. Therefore, from the total number of samples in the Monte Carlo simulation, only those samples that reconcile the response to an inflation and to an air-puff test to be within the experimental ranges[1, 45, 5] were considered. After including this exclusion criteria, only the 29% (1127 over 3855) of the Healthy cases, the 30.5% (1327 over 4344) of the KTC cases, and the 21.5% (219 over 1017) of the LASIK cases were included in the training dataset. The bright areas in Fig.2.c(1–3) (Healthy: red; KTC: blue; LASIK: green) show the response to the air-puff for the admitted samples.

The empirical distribution of the material parameters related to the matrix (D_1 and D_2) did not follow a uniform distribution whereas those related to the fibres (k_1 and k_2) were found to be uniformly distributed (see in A.6 in Appendix A). A Kolmogorov–Smirnov test shows non significant differences between the material parameters of the Healthy–LASIK and the KTC–LASIK populations (see in Table 2). On the contrary, significant differences were found for D_1 and D_2 between the Healthy–KTC populations.

When the cornea is under the action of the IOP (i.e. its physiological stress state), the cornea is under a pure traction membrane stress state where the full cornea works in tension (i.e. both extracellular matrix and both families of collagen fibres) and, therefore, no bending effects exists. However, during an air-puff, the cornea experiences bending. While the anterior surface goes from a traction state of stress to a compression state of stress, the posterior surface works in tension. Hence, in the anterior corneal stroma the collagen fibres are not collaborating to load bearing since they do not support buckling and the stiffness of the cornea mainly relies on the

Table 2: **Kolmogorov–Smirnov Hypothesis Test between Populations regarding the Material Parameters.**

	D_1		D_2		k_1		k_2	
Comparison	**h**	**p–value**	**h**	**p–value**	**h**	**p–value**	**h**	**p–value**
Healthy–KTC	1	<0.001	0	0.058	0	0.328	0	0.983
Healthy–LASIK	0	0.869	0	0.779	0	0.584	0	0.482
KTC–LASIK	0	0.098	0	0.161	0	0.681	0	0.725

Table Legend. **h**: indicates the result of the hypothesis test (i.e. h=1 rejects the null hypothesis that both populations come from the same continuous probability distribution); **p–value**: asymptotic p–value of the test (i.e. p–value < 0.05 means that the null hypothesis can be rejected at a 5% of significance level) .

extracellular matrix. At the same time, the collagen fibres on the posterior stroma suffer from a higher elongation, resulting on an overall non-physiological state of stress. In this regard, due to the action of the IOP, no significant differences in the maximum principal stress and in the maximum principal stretch were observed between the different populations for both, the anterior and posterior corneal surfaces. On the contrary, when the maximum principal stress and stretch are compared at the instant of maximum corneal displacement, significant statistical differences between all populations were found at the posterior surface (see Table 3). However, at the anterior surface, significant differences were found only for the maximum principal stretch, whereas for the maximum principal stress, differences were found only between Healthy and KTC populations (see Table 3).

Table 3: **Kolmogorov–Smirnov Hypothesis Test between Populations regarding the Stress–Strain Apical behavior.**

	Anterior				**Posterior**			
	Stretch		**Stress**		**Stretch**		**Stress**	
Comparison	**h**	**p–value**	**h**	**p–value**	**h**	**p–value**	**h**	**p–value**
Healthy–KTC	1	<0.001	1	<0.001	1	<0.001	1	<0.001
Healthy–LASIK	1	<0.001	0	0.073	1	<0.001	1	<0.001
KTC–LASIK	1	<0.001	0	0.083	1	<0.001	1	0.049

Table Legend. **h**: indicates the result of the hypothesis test (i.e. h=1 rejects the null hypothesis that both populations come from the same continuous probability distribution); **p–value**: asymptotic p–value of the test (i.e. p–value < 0.05 means that the null hypothesis can be rejected at a 5% of significance level) .

3.2. Sensitivity Analysis

The sensitivity and ANOVA analysis conducted on the dataset (with the admitted samples only) demonstrates the predominant role of the material parameters on U_{num} (see in Fig.3.a). For the whole population, the ANOVA analysis showed that the most influential parameters are the material parameters (D_1 and D_2), followed by the IOP and the central corneal thickness (CCT). When the populations are considered separately (Fig.3.b and Fig.3.c respectively) the general trends are kept for the Healthy and LASIK populations. However, for the KTC population, the IOP seems to play a more important role than the material itself. In addition, the Superior–Inferior Curvature slightly influences the numerical response for the KTC population. The results demonstrate the significant importance of the IOP on U for those cases where the corneal thickness is lower with respect to the healthy case (i.e. KTC and LASIK).

Figure 3: **Pareto chart representing the variables responsible for the 95% of the mechanical response (displacement). (a)** Impact of the main variables on the mechanical response taking into account the whole dataset; **(b)** Impact of the main variables on the mechanical response taking into account the Healthy cases of the dataset; **(c)** Impact of the main variables on the mechanical response taking into account the KTC cases of the dataset; **(d)** Impact of the main variables on the mechanical response taking into account the LASIK cases of the dataset. *Legend:* intraocular pressure (IOP), central corneal thickness (CCT), Superior–Inferior Curvature of the eye (R_v), material parameters (D_1, D_2 and k_2) and interaction between material parameter D_1 and the intraocular pressure ($D_1 : IOP$).

In general, the sensitivity analysis showed that the most influential parameters on the displacement response (U_{num}) were: the material parameters (D_1, D_2 and k_2), the intraocular pressure (IOP), and the central corneal thickness (CCT) in all populations. An exception is found for the Superior–Inferior Curvature (R_V) for the KTC population. However, the most remarkable result is the negligible impact of the material parameter k_1 on the numerical response. Although k_1 cannot be removed from the simulations since it is a material parameter of the strain energy function (1) , the result from the sensitivity analysis suggests that setting its value to its average (i.e. $k_1 = 19$ [kPa]) seems to be a reasonable choice in terms of developing the material predictors. Henceforth, k_1 parameter is treated as a constant value avoiding the necessity of adjusting or training an specific model for it, with the consequent reduction in computational cost.

3.3. Response surface predictor models (MLP, SVR and QRS)

According to the results from the sensitivity analysis, the predictive models were built considering: D_1, D_2, k_2, IOP, CCT, and U_{num}, following the methodology described in *Material and Methods*. Table 4 shows the main results from the fitting for the three models under consideration.

Table 4: **Accuracy for the four predictors (MLP: Multiple Layer Perceptron; SVR: Support Vector Regressor; SR: Surface Response) for the different populations (Healthy, KTC and LASIK)**

D_1									
	Healthy			**KTC**			**LASIK**		
Var	**MLP**	**SVR**	**QRS**	**MLP**	**SVR**	**QRS**	**MLP**	**SVR**	**QRS**
$\mathbf{R^2}$	0.967	0.958	0.952	0.886	0.869	0.843	0.954	0.948	0.949
AIC	-1769	-1661	-1671	-1386	-1324	-1241	-404	-391	-396
μ_{res}	-0.002	-0.005	-0.002	0.000	0.002	0.001	-0.003	-0.003	0.000
σ_{res}	0.028	0.032	0.032	0.054	0.058	0.063	0.028	0.030	0.030
D_2									
	Healthy			**KTC**			**LASIK**		
Var	**MLP**	**SVR**	**QRS**	**MLP**	**SVR**	**QRS**	**MLP**	**SVR**	**QRS**
$\mathbf{R^2}$	0.962	0.954	0.952	0.905	0.897	0.864	0.963	0.968	0.956
AIC	2589	2663	2626	3302	3339	3467	600	584	613
μ_{res}	-0.295	-0.622	-0.312	0.165	0.193	-0.083	0.312	0.171	0.498
σ_{res}	5.408	5.912	5.653	8.273	8.606	9.874	5.043	4.656	5.413
k_2									
	Healthy			**KTC**			**LASIK**		
Var	**MLP**	**SVR**	**QRS**	**MLP**	**SVR**	**QRS**	**MLP**	**SVR**	**QRS**
$\mathbf{R^2}$	0.857	0.822	0.781	0.563	0.518	0.432	0.817	0.806	0.774
AIC	5337	5421	5464	6360	6411	6477	1289	1295	1308
μ_{res}	-10.970	-23.592	-18.253	-3.106	-8.900	-10.458	-7.413	-13.408	-10.401
σ_{res}	148.2	164.0	172.6	220.1	232.4	249.4	176.1	181.4	194.5

Table Legend. $\mathbf{R^2}$: coefficient of determination; **AIC**: Akaike Information Criterion for the final adjusted model; μ_{res}: average of the residuals of the predicted response with respect the expected response; σ_{res}: standard deviation of the residuals of the predicted response with respect to the expected response.

All response surface methods perform similarly, though the MLP model showed a slightly better performance (see R^2 value in Table 4). All models (D_1, D_2, and k_2) presented a good coefficient of determination (R^2) and a relative low dispersion of the residuals (i.e. predicted response minus real response) with their mean around zero with exception of k_2 which presented a higher dispersion. This result was somehow expected since D_1 and D_2 were the material parameters to which the corneal displacement was more sensitive. In general, the best fitting always corresponded to the Healthy population, whereas the worst performance was always found for the LASIK population. These results could be thought to be related with the disruption of the

collagen fibres due to the corneal flap generated during the surgery and its consequent loss of stiffness. However, since our models are phenomenological and not structural, the dispersion is thought to be mainly associated with the abrupt change of the corneal curvature of the anterior surface due to the resultant flattened area induced by the surgery and the dispersion on the central corneal thickness. As mentioned in the *Materials and Methods* section, in addition to individual predictors of the material parameters for each of the populations, a predictor was fitted for each material parameter but considering the entire dataset. No significant differences in the results where obtained when compared with predictors build for individual populations (results not shown). Therefore, in what follows, only results corresponding to individual populations will be shown.

Regarding the Akaike Information Criterion, it remains almost constant between methods (MLP, SVR and QSR) for the same parameter (D_1, D_2 and k_2), indicating that all models obtained similar quality on the adjustment. The residual analysis indicates that the best predictions (i.e. mean close to 0) belong always to the D_1 independently of the method and the population. On the contrary, the worst predictions was always associated with k_2 independently of the method and the population. However, it is remarkable that Healthy population showed the best accuracy with respect to the rest of the populations, whereas the KTC showed the worst accuracy. This finding could have an explanation on the inherent geometrical variability of the keratoconus. For this pathology, the location of the disease is not repeatable among patients, leading to a very heterogeneous distribution of geometrical features among patients. On the contrary, geometrical features of healthy eyes are more repeatable. Furthermore, the better accuracy of the D_1 and the D_2 parameters are directly supported by their importance on the corneal response of the model (see in Fig.3).

3.4. Neighborhood-Based protocol (K-nn search)

The K-nn Search method does not required the fitting of a particular mathematical function to predict the material parameters in terms of the corneal patient's geometric data and the mechanical response to the air-puff since it simply searches for the closest point in the data base

to the patients data (IOP, CCT and U). However, this method helps to demonstrate the inherent coupling existing between CCT, IOP and U that has been demonstrated in previous studies [2].

Figure 4: **Coupled Effect of the Corneal Response (Patient h_0, Table 1).** All the healthy cases of the dataset are represented as blue dots in the figures. The biomarkers selected for determining the mechanical properties of the eye are shown to outline the coupling between different parameters: different combinations of thickness, material and intraocular pressure could lead to the same displacement. **(a)** Displacement (U) versus Thickness (CCT) considering constant the Intraocular Pressure (IOP=12 mmHg). In red dots all the feasible combinations of CCT that lead to the same displacement (1 mm) when the material properties and the pressure are fixed; **(b)** Displacement (U) versus IOP (IOP) considering constant the Thickness (CCT=578 microns). In red dots all the feasible combinations of IOP that lead to the same displacement (1 mm) when the material properties and the CCT is fixed; **(c)** Intraocular Pressure (IOP) versus Thickness (CCT) considering constant the Displacement (U=1.00 mm). All tuples of IOP and CCT that can lead to the same displacement (1 mm). The dispersion of the parameters are only influenced by the tissue stiffness, i.e. the lowest pressures and thickness only can behave as the highest pressures and thickness if the material properties are stiffer. In this vein, although different corneas could have a close average tissue stiffness, an increment on IOP or CCT could lead to a less compliant mechanical response.

Figure 4a show that for a given value of the IOP, different combinations of the material properties and corneal thickness lead to the same corneal displacement, U, (see red dots in Fig. 4a). Similarly, for a given corneal thickness, different combinations of material parameters and IOP give the same corneal displacement to an air-puff (see in Fig.4.b). This result shows that different combinations of material parameters, IOP and CCT can lead to the same corneal displacement, U, making impossible to quantify each contribution separately. However, when the patient specific information (IOP, CCT, and U) is used as input to the dataset (red triangle in Fig.4.c), it is possible to define a neighborhood of feasible points around the patient's data (blue diamonds in Fig.4.c) from which the material parameters can be estimated. This method is the most straightforward in terms of searching and implementation, as well as the one giving the best prediction (see next section). However, it is also the most expensive in terms of computations since the accuracy of the method is highly affected by the resolution of the grid used for the dataset (number of samples present in the dataset).

3.5. Examples with clinical data

Table 5 shows the material model parameters predictions for the 5 patients described in Table 1. All the material model parameters obtained with the different predictors were used to simulate a non-contact tonometry test using the patient's specific data available on each case i.e., topography of the cornea and IOP. For most cases, the predicted displacements (U_{num}) was in close

Table 5: **Validation using a priori unknown Clinical Patient Data (Table 1). Application of the former patient–specific geometrical reconstruction algorithm [4] coupled with the present patient–specific material prediction methodology to reproduce the maximum deformation amplitude (displacement) of the corneal apex when subjected to a Non–Contact Tonometry test (clinical values corresponds to CorVis measurement system).**

		Input	Output	Validation	
			$\mathbf{D_1}$ | $\mathbf{D_2}$ | $\mathbf{k_1}$ | $\mathbf{k_2}$	$\mathbf{U_{num}}$	$\epsilon(\%)$
L.	**Meth.**		[kPa] | [–] | [kPa] | [–]	[mm]	[–]
h_0	K-nn	IOP=12 mmHg CCT=578 μm U=1.00 mm	0.277 | 120.6 | 20.8 | 516.9	1.007	0.726
	QRS		0.193 | 138.3 | 19.0 | 545.6	1.013	1.251
	MLP		0.446 | 85.7 | 19.0 | 843.1	1.022	2.158
	SVR		0.292 | 122.8 | 19.0 | 191.5	1.006	0.573
ktc_0	K-nn	IOP=15 mmHg CCT=545 μm U=1.12 mm	0.267 | 103.5 | 17.9 | 525.3	1.153	2.968
	QRS		0.289 | 97.9 | 19.0 | 455.5	1.175	4.917
	MLP		0.379 | 80.6 | 19.0 | 644.6	1.174	4.814
	SVR		0.368 | 81.3 | 19.0 | 687.4	1.171	4.503
ktc_1	K-nn	IOP=15 mmHg CCT=544 μm U=1.03 mm	0.330 | 109.0 | 17.6 | 374.5	1.025	0.529
	QRS		0.320 | 105.9 | 19.0 | 458.4	1.042	1.150
	MLP		0.186 | 131.3 | 19.0 | 443.0	1.072	4.099
	SVR		0.229 | 127.2 | 19.0 | 321.1	1.042	1.147
ktc_2	K-nn	IOP=15 mmHg CCT=464 μm U=1.05 mm	0.385 | 126.7 | 20.8 | 267.5	1.161	10.565
	QRS		0.363 | 122.0 | 19.0 | 540.0	1.186	12.964
	MLP		0.379 | 128.1 | 19.0 | 412.8	1.149	9.408
	SVR		0.365 | 126.1 | 19.0 | 423.3	1.175	11.857
ktc_3	K-nn	IOP=16 mmHg CCT=460 μm U=1.12 mm	0.388 | 120.5 | 18.5 | 592.7	1.131	0.940
	QRS		0.319 | 115.3 | 19.0 | 515.3	1.238	10.545
	MLP		0.336 | 122.1 | 19.0 | 397.0	1.198	6.933
	SVR		0.330 | 116.2 | 19.0 | 486.6	1.227	9.533

Table Legend. ($\mathbf{D_1}$ [kPa] | $\mathbf{D_2}$ [–] | $\mathbf{k_1}$ [kPa] | $\mathbf{k_2}$ [–]): Parameters of the Demiray + G–H–O energy strain function ; $\mathbf{U_{num}}$ [mm]: maximum deformation amplitude provided by the numerical simulation of the non–contact tonometer; $\epsilon(\%) = |U_{num} - U|/U \cdot 100$: percentage difference between numeric and clinical displacement.

proximity to the measured displacement (U), being the largest error difference, $\epsilon(\%)$, a 13% for the KTC eye (patient ktc2) and the QRS method. In addition, although local minima exist, and we are aware of them, material predictions associated with local minima also lead to a predicted corneal displacement close to the actual measurements (results not shown). For patient ktc2, for which the material predictions lead to the worst corneal displacement predictions, it was found that the closest neighbor to the Patient's data was located at a distance that was an order of magnitude larger than for the other patients. This indicates the need for a larger number of samples in the dataset, i.e., a more dense sampling of the parameters space. However, it is worth mentioning

that, as the number of patients in the data base increases, the prediction capabilities of all models will also increase in general. Further information regarding the performance of each methods can be found in Appendix A. Regarding the time required to search a set of material parameters (t_{exec}, Table A.6), the fastest method is the K–nn Search since it does not require of any iterative procedure to find the material properties. In addition, depending on the initial material seed, the iterative procedure may found different minima and take longer execution times. For these reason, the implementation of the Algorithm includes a multiple seed strategy in order to identify the material parameters with minimum possible error.

4. Conclusions

A series of mathematical models have been proposed to predict the mechanical properties of corneal tissue from patient's specific data obtained by means of a non-contact tonometry test. The proposed methodology is based on *in-silico* simulations of the non-contact tonometry tests using patients specific corneal geometry data [4]. The methodology is amenable for implementation on commercial devices for clinical applications, and provides acceptable execution times and accuracy.

The computational simulation has different assumptions of the material and the modelling that cannot be neglected. First, we used a phenomenological and macroscopic material model for the cornea that allows to reproduce, within the experimental reported range, the corneal response to both, inflation to increase values of IOP, and the corneal displacement induced by a non–contact tonometry test. Regarding the material model, there are some hypothesis that must be addressed such as the absence of viscoelasticity or the use of a generic orthogonal pattern of fibers following the proposed by Meek et al. (2009) [50]. With respect to the viscoelastic properties of the cornea, the loading of the tissue is fast enough as to consider that viscoelastic effects do not playing a major role on the corneal response [46]. This assumption has been widely accepted in former publications (see several Elsheikh, Pandolfi, Lanchares or Studer) and, lately, Simonini et al. (2016) [56] have reported a study on the dynamic of the cornea when subjected to an air-puff that suggests the great importance of the elastic contribution of the stroma during the loading

phase of the air-jet, but the minor contribution of the inertia and viscoelasticity. However, if the recovery of the cornea during the unloading phase would be addressed, the inclusion of inertia and viscoelasticity would be essential. Concerning, the pattern of collagen fibres is not a patient-specific since it is not yet easily accessible. Although Winkler et al. and others authors have reported a more precise micro-structural distribution of the fibres using SHG optical microscopy [51, 52, 53, 47, 48, 49], the inclusion of the patient-specific micro-structural information of the cornea would not be useful but increasing the computation costs and introducing a new bias since this information was not accessible for our patients. Nevertheless, the proposed methodology does not prevent the use of more complex material models that incorporate information of the micro-structure of the cornea, viscoelasticity or inertia. Second, the boundary condition simulating the air-jet impact has been assumed as a constant pressure applied over the cornea. Although for computing the pressure pattern a CFD analysis has been applied over a generic cornea, a more precise simulation would require of a fluid structure simulation since the corneal geometry and the deformation of the cornea over the time may have an important impact on the pressure transferred during the air-puff.

In spite of its considerable computational cost, the Monte Carlo simulation has proven to be a powerful tool to be used for real–time estimation of the corneal mechanical properties from a non-contact tonometry test on the clinic. In addition, the mathematical tools (MLP, SVR and QRS) have shown a good performance on predicting the corneal material parameters, but the inherent coupling between the IOP, the CCT, and the corneal mechanical properties affecting the corneal response, introduces an unavoidable dispersion on the data that reduces the performance of these methods. In this regard, the K–nn Search has proved to be the most reliable method. Since it restricts the search to the neighborhood of the patient, the method is not prone to find local minima as well as it shows the best performance in terms of execution time. Further, the material model parameters predicted with by K-nn search method lead to the most accurate predictions of the corneal displacement with respect to the clinical value (i.e. less than 3% difference with respect to the clinical results). Despite the fact that the main drawback is the considerable computational cost involved in generating the dataset as it needs a fine resolution

on the data grid for good accuracy, it is still more suitable than other optimization methods such as the IFEM thanks to its real-time response (i.e. no finite element computation is required for the diagnosis but the patient can be used subsequently for updating the dataset).

No significant differences have been found between populations, in general, in terms of the material parameters. In this regard, only Healthy and KTC populations showed significant differences in terms of D_1 and D_2 parameters but not in terms of k_1 and k_2. Therefore, these results indicate that considering differences on the material parameters of the cornea may not be sufficient to classify healthy and keratoconus eyes using a single air-puff test, pointing out to the necessity of having more than a single test for characterizing properly the properties of the eye. However, till now, there is no additional in-vivo test that allows complementing the air-puff diagnosis and the results should be assessed additionally by, for example, ex-vivo inflation tests, as we used for constraining the search of material properties with both physiological behaviours (i.e. inflation and air-puff). Besides, our results suggest that variations in corneal thickness may be a more reliable monitoring variable in terms of classifying the healthy from the KTC population. In addition, based on the finite element simulations, the maximum principal stretch in the anterior and posterior surfaces of the corneal obtained at the instant of maximum corneal deformation may be used as discriminant to classify different groups (Healthy, KTC and LASIK).

One final limitation regarding the clinical biomarkers used for the prediction must be tackled. For the sake of simplicity, only 3 clinical biomarkers have been used for predicting the material properties of the cornea: pressure (i.e. the IOP), geometry (i.e. CCT) and displacement (i.e. the maximum deformation amplitude of the CorVis test). Since our models are mainly phenomenological, macroscopic and are not taking into account the inertia, viscoelasticity and micro-structural features of the cornea, the dynamic parameters given by the CorVis diagnosis test cannot be trustworthily used. Besides, the ANOVA and Pareto analysis showed that, for the models used in the present study, the most influential parameters were the selected one. However, this is no problem whatsoever for easily introducing other corneal parameters in the predictive model, provided that they can be accurately measured in both, the experimental and the numerical results. Although only these 3 biomarkers have been used, the methodology has

been tested with actual unknown patient data that did not form part of the dataset. The predicted material parameters, along with the patient's corneal geometry and IOP were used to simulate a non–contact tonometry test to predict the corneal displacement. The numerical results resulted in errors of less than 10% in most cases, with the K-nn search methodology outperforming the response surface based methods achieving errors of less than 3%.

The important remark of the present study is that the proposed methodology, independently of the complexity of the numerical simulations, is amenable for real–time diagnosis and implementation in commercial devices. Importantly, it allows easily introducing additional elements (e.g. viscoelasticity, microstructure, dynamics...) that could enhance the performance and accuracy of the results without modifying the underlying methodology. Eventually, the computational framework incorporated actual clinical data (corneal topographies, IOP and corneal apical displacement from a non–contact tonometry test) to predict the mechanical properties of the corneal. These results could be used for surgical planning, or to monitor the evolution of a given patient by looking at changes in the mechanical properties with time.

Acknowledgement

Special thanks to Dr. Joaquin Fernandez at the Qvision Ophthalmic Unit of the Vithas Virgen del Mar Hospital (Almeria, Spain) for prospectively collecting the validation data.

Funding

The research leading to these results has received funding from the European Union's Seven Framework Program managed by REA Research Executive agency http://ec.europa.eu/research/rea (FP7/2007-2013) under Grant Agreement FP7-SME-2013 606634, the Spanish Ministry of Economy and Competitiveness under the Grant Agreement DPI2014-54981R, the Government of Aragón (predoctoral contract of the author), the Ibercaja-CAI mobility program (mobility funding for research stay of the author) and the Swiss Federal Department of Economic Affairs, Education and Research (Federal Commission for Scholarships for Foreign Students).

Appendix A. Additional Results

This appendix contains the extended non-essential results but needed to understand the complete scope of the outcomes. The extensions are related to:

- **Sensitivity Analysis**: the Response Surface ($U = f(geometry, pressure, material)$) used for analysing the impact of the different variables (geometry, pressure and material) to the numerical variable under analysis in the FE computation (displacement) is depicted in Fig.A.5.

- **Statistical distribution of the mechanical properties of the cornea for the Monte Carlo simulation**: all the Monte Carlo combinations of material that fulfil both physiological responses (inflation and air-puff) are gathered in Fig.A.6 (green histogram). While the parameters related to the fibres are uniformly distributed (k_1 and k_2), the matrix parameters (D_1 and D_2) stack around 0.4–0.45 [kPa] and [130–140].

- **Accuracy of the prediction after the training phase for the SVR and MLP**: the accuracy of the predictions of both methods after the training phase is depicted in Fig.A.7. Support Vector Regressor does not present blue shaded zone since only one SVR is used. On the contrary, the MLP uses 7 different assemblies and, afterwards, computes the average. Therefore, the confidence intervals (blue shaded zones) can be established.

- **Goodness of the fitting for the SVR, MLP and QRS models**: correlation plot of the predicted property versus the actual value in the dataset is depicted in Fig.A.8. Material properties D_1 and D_2 show the best model fitting whereas k_2 shows a higher dispersion (k_1 is not shown since it was discarded after the sensitivity analysis).

- **Additional Performance of the methodology**: results of supplementary performance variables (execution time, distance of the nearest neighbor and initial tangent modulus) are depicted in Table A.6.

Figure A.5: **Slice plots of the Quadratic Response Surface for each population (Healthy–red, KTC–blue, LASIK–green).** The slice plots show the individual contribution of the different model parameters on the numerical displacement. The higher the slope, the higher the contribution (shaded zones represents the standard deviation of the parameter whereas solid lines represent the mean response). **(a)** Impact of the model parameters on the numerical displacement of the Healthy population; **(b)** Impact of the model parameters on the numerical displacement of the KTC population; **(c)** Impact of the model parameters on the numerical displacement of the LASIK population

Figure A.6: **Statistical distribution of the mechanical properties of the cornea for the Monte Carlo simulation.** The empirical distribution (green histogram) due to all the combinations of material parameters that fulfil both physiological behaviours (inflation and air-puff) shows that the fibre's parameters are uniformly distributed.

Figure A.7: **MLP (right panel) and SVR (left panel) predictions for validating the training phase (only Healthy response is shown). a.(1–3)**: D_1, D_2 and k_2 predictions depending on the patient case for the MLP method. Blue intervals correspond to the Confidence Interval (95% light blue and 99% dark blue) of the prediction, since the method is composed of an ensemble of 7 independent MLP and the response is the average of each independent MLP; **b.(1–3)**: D_1, D_2 and k_2 predictions depending on the patient case for the SVR method. k_1 predictor is not computed since it has been discarded after the sensitivity analysis.

Figure A.8: **Correlation plot of the Predicted Parameter (y-axis) vs Expected Parameter (x-axis) for the Healthy group. a.(1–3)**: QRS; **b.(1–3)**: MLP; **c.(1–3)**: SVR. D_1 and D_2 show a good prediction of the values whereas k_2 presents a higher dispersion. k_1 predictor is not computed since it has been discarded after the sensitivity analysis.

Table A.6: **Performance of the Prediction of the Patient–Specific Material Properties for the Clinical Patients (Table 1) Applying the Prediction Models (K-nn Search: neighbors-based prediction model; QRS: Quadratic Response Surface model; MLP: Multiple Layer Perceptron; SVR: Support Vector Regressor)**

		$\mathbf{t_{exec}}$	**Dist.**	**E**	**E (%)**
L.	**Meth.**	[s]	[–]	[kPa]	[–]
h_0	K-nn	0.060 ± 0.023	0.003	283.637	–
	QRS	1.996 ± 0.562	–	236.15	-16.7
	MLP	19.282 ± 9.551	–	305.333	7.7
	SVR	75.304 ± 4.469	–	291.146	2.7
ktc_0	K-nn	0.036 ± 0.002	0.006	237.407	–
	QRS	1.145 ± 0.101	–	245.760	3.5
	MLP	14.473 ± 1.458	–	259.284	9.2
	SVR	7.833 ± 4.724	–	255.510	7.6
ktc_1	K-nn	0.036 ± 0.003	0.005	286.22	–
	QRS	0.781 ± 0.028	–	279.328	-2.4
	MLP	17.861 ± 2.922	–	222.531	-22.3
	SVR	10.130 ± 2.168	–	250.773	-12.4
ktc_2	K-nn	0.0336 ± 0.003	0.025	375.877	–
	QRS	0.460 ± 0.015	–	341.716	-9.1
	MLP	4.962 ± 0.238	–	367.299	-2.3
	SVR	2.284 ± 0.187	–	352.159	-6.3
ktc_3	K-nn	0.035 ± 0.003	0.006	354.524	–
	QRS	0.519 ± 0.018	–	296.684	-16.3
	MLP	7.892 ± 0.160	–	322.154	-9.1
	SVR	4.091 ± 0.269	–	306.076	-13.7

Table Legend. $\mathbf{t_{exec}}$ [s]: execution time for prediction; **Dist. [–]**: minimum distance of the neighborhood (only for K-nn Search); $\mathbf{E} = 6 \cdot D_1 D_2 + 4 \cdot k_1$ [kPa]: Equivalent Initial Tangent Modulus ($\lambda = 1$); $\mathbf{E}(\%) = 100 \cdot (1 - E_j / E_{K-nn})$: initial slope difference between the Equivalent Initial Tangent Modulus of the *'j'* Method (E_j), where *'j'* are QRS, MLP, and SVR, with respect to the Equivalent Initial Tangent Modulus of the K-nn Search Method (E_{K-nn}).

[1] M. Lanza, S. Iaccarino, M. Bifani, In vivo human corneal deformation analysis with a scheimpflug camera, a critical review., J. Biophotonics 9(5) (2016) 464–477.

[2] M. Á. Ariza-Gracia, J. F. Zurita, D. P. Piñero, J. F. Rodriguez-Matas, B. Calvo, Coupled biomechanical response of the cornea assessed by non-contact tonometry. a simulation study, PLoS One 10 (3) (2015) e0121486.

[3] A. Sinha Roy, M. Kurian, H. Matalia, R. Shetty, Air-puff associated quantification of non-linear biomechanical properties of the human cornea in vivo, J. Mech. Behav. Biomed. Mater. 48 (2015) 173–182.

[4] M. Á. Ariza-Gracia, J. Zurita, D. P. Piñero, B. Calvo, J. F. Rodríguez-Matas, Automatized patient-specific methodology for numerical determination of biomechanical corneal response, Ann. Biomed. Eng. 44(5) (2016) 1753–1772.

[5] Z. Hassan, L. Modis, Jr, E. Szalai, A. Berta, G. Nemeth, Examination of ocular biomechanics with a new scheimpflug technology after corneal refractive surgery, Cont. Lens Anter. Eye 37(5) (2014) 337–341.

[6] F. Faria-Correia, I. Ramos, B. Valbon, A. Luz, C. J. Roberts, R. Ambrósio, Jr, Scheimpflug-based tomography and biomechanical assessment in pressure-induced stromal keratopathy, J. Refract. Surg. 29 (5) (2013) 356–358.

[7] Y. Hon, A. K. C. Lam, Corneal deformation measurement using scheimpflug noncontact tonometry, Optom. Vis. Sci. 90 (1) (2013) e1–e8.

[8] J. Hong, J. Xu, A. Wei, S. X. Deng, X. Cui, X. Yu, X. Sun, A new tonometer–the corvis st tonometer: clinical comparison with noncontact and goldmann applanation tonometers, Invest. Ophthalmol. Vis. Sci. 54 (1) (2013) 659–665.

[9] S. Kling, S. Marcos, Contributing factors to corneal deformation in air puff measurements, Invest. Ophthalmol. Vis. Sci. 54 (7) (2013) 5078–5085.

[10] C. J. Roberts, Concepts and misconceptions in corneal biomechanics, J. Cataract Refract. Surg. 40 (6) (2014) 862–869.

[11] P. M. Pinsky, D. V. Datye, A microstructurally-based finite element model of the incised human cornea, J. Biomech. 24 (10) (1991) 907–922.

[12] P. M. Pinsky, D. van der Heide, D. Chernyak, Computational modeling of mechanical anisotropy in the cornea and sclera, J. Cataract Refract. Surg. 31 (1) (2005) 136–145.

[13] M. Lago, M. Rupérez, F. Martínez-Martínez, C. Monserrat, E. Larra, J. Güell, C. Peris-Martínez, A new methodology for the in vivo estimation of the elastic constants that characterize the patient-specific biomechanical behavior of the human cornea, J. Biomech. 48 (1) (2015) 38–43.

[14] A. Pandolfi, F. Manganiello, A model for the human cornea: constitutive formulation and numerical analysis, Biomech. Model. Mechanobiol. 5 (4) (2006) 237–246.

[15] A. Pandolfi, G. A. Holzapfel, Three-dimensional modeling and computational analysis of the human cornea considering distributed collagen fibril orientations, J. Biomech. Eng. 130 (6) (2008) 061006.

[16] E. Lanchares, B. Calvo, J. A. Cristóbal, M. Doblaré, Finite element simulation of arcuates for astigmatism correction, J. Biomech. 41 (4) (2008) 797–805

[17] H. P. Studer, H. Riedwyl, C. A. Amstutz, J. V. M. Hanson, P. Büchler, Patient-specific finite-element simulation of

the human cornea: a clinical validation study on cataract surgery, J. Biomech. 46 (4) (2013) 751–758.

[18] F. Bao, M. Deng, Q. Wang, J. Huang, J. Yang, C. Whitford, B. Geraghty, A. Yu, A. Elsheikh,Evaluation of the relationship of corneal biomechanical metrics with physical intraocular pressure and central corneal thickness in ex vivo rabbit eye globes, Exp. Eye Res. 137 (2015) 11–17.

[19] Kok, Schalk and Botha, Natasha and Inglis, Helen M, Calibrating corneal material model parameters using only inflation data: An ill-posed problem, International Journal of Numerical Methods in Biomedical Engineering, 30:12 (2014) 1460–1475

[20] Girard, Michaël J A. and Downs, J Crawford and Bottlang, Michael and Burgoyne, Claude F. and Suh, J-K Francis., Peripapillary and posterior scleral mechanics–part II: experimental and inverse finite element characterization., J Biomech Eng, 131:5 (2009) DOI: 10.1115/1.3113683

[21] Girard, Michaël J A. and Downs, J Crawford and Burgoyne, Claude F. and Suh, J-K Francis., Peripapillary and posterior scleral mechanics–part I: development of an anisotropic hyperelastic constitutive model., J Biomech Eng, 131:5 (2009), DOI: 10.1115/1.3113682

[22] Nguyen, T. D. and Boyce, B. L., An inverse finite element method for determining the anisotropic properties of the cornea., Biomech Model Mechanobiol, 10:3 (2011) 323–337 DOI: 10.1007/s10237-010-0237-3

[23] A. Elsheikh, A. Joda, A. Abass, D. Garway-Heath, Assessment of the ocular response analyzer as an instrument for measurement of intraocular pressure and corneal biomechanics, Curr. Eye Res. 40 (11) (2015) 1111–1119.

[24] C. Whitford, H. Studer, C. Boote, K. M. Meek, A. Elsheikh, Biomechanical model of the human cornea: considering shear stiffness and regional variation of collagen anisotropy and density, J. Mech. Behav. Biomed. Mater. 42 (2015) 76–87.

[25] E. Lanchares, M. A. del Buey, J. A. Cristóbal, L. Lavilla, B. Calvo, Biomechanical property analysis after corneal collagen cross-linking in relation to ultraviolet a irradiation time, Graefes Arch. Clin. Exp. Ophthalmol 249 (8) (2011) 1223–1227.

[26] R. Navarro, F. Palos, E. Lanchares, B. Calvo, J. A. Cristóbal, Lower- and higher-order aberrations predicted by an optomechanical model of arcuate keratotomy for astigmatism, J. Cataract Refract. Surg. 35 (1) (2009) 158–165.

[27] A. S. Roy, W. J. Dupps, Jr, Patient-specific modeling of corneal refractive surgery outcomes and inverse estimation of elastic property changes, J. Biomech. Eng. 133 (1) (2011) 011002.

[28] S. Kling, N. Bekesi, C. Dorronsoro, D. Pascual, S. Marcos, Corneal viscoelastic properties from finite-element analysis of in vivo air-puff deformation, PLoS One 9 (8) (2014) e104904.

[29] F. Boschetti, V. Triacca, L. Spinelli, A. Pandolfi, Mechanical characterization of porcine corneas, J. Biomech. Eng. 134(3) (2012) 031003.

[30] J.-D. Ho, C.-Y. Tsai, R. J.-F. Tsai, L.-L. Kuo, I.-L. Tsai, S.-W. Liou, Validity of the keratometric index: evaluation by the pentacam rotating scheimpflug camera, J. Cataract. Refract. Surg. 34 (1) (2008) 137–145.

[31] D. Smadja, D. Touboul, A. Cohen, E. Doveh, M. R. Santhiago, G. R. Mello, R. R. Krueger, J. Colin, Detection of subclinical keratoconus using an automated decision tree classification, Am. J. Ophthalmol. 156 (2) (2013)

687 237–246.e1.

688 [32] M. A. Valdés-Mas, J. D. Martín-Guerrero, M. J. Rupérez, F. Pastor, C. Dualde, C. Monserrat, C. Peris-Martínez,
689 A new approach based on machine learning for predicting corneal curvature (k1) and astigmatism in patients with
690 keratoconus after intracorneal ring implantation, Comput. Meth. Prog. Bio. 116 (1) (2014) 39–47.

691 [33] P. A. Accardo, S. Pensiero, Neural network-based system for early keratoconus detection from corneal topography,
692 J. Biomed. Inform. 35 (3) (2002) 151–159.

693 [34] M. C. Arbelaez, F. Versaci, G. Vestri, P. Barboni, G. Savini, Use of a support vector machine for keratoconus and
694 subclinical keratoconus detection by topographic and tomographic data, Ophthalmology 119 (11) (2012) 2231–
695 2238.

696 [35] E. Soudah, J. F. Rodriguez, R. Lopez, Mechanical stress in abdominal aortic aneurysms using artificial neural
697 networks, J. Mech. Med. Biol. 15 (03) (2015) 1550029.

698 [36] E. Businaro, H. Studer, B. Pajic, P. Büchler, Gaussian process prediction of the stress-free configuration of pre-
699 deformed soft tissues: Application to the human cornea, Med. Eng. Phys. 38 (4) (2016) 339–345.

700 [37] J. Krenek, K. Kuca, A. Bartuskova, O. Krejcar, P. Maresova, V. Sobeslav, Artificial neural networks in biomedicine
701 applications, in: Proceedings of the 4th International Conference on Computer Engineering and Networks,
702 Springer, 2015, pp. 133–139.

703 [38] M. R. Bryant, P. J. McDonnell, Constitutive laws for biomechanical modeling of refractive surgery,
704 J. Biomech. Eng. 118 (4) (1996) 473–481.

705 [39] Y. S. Rabinowitz, Keratoconus, Surv. Ophthalmol. 42 (4) (1998) 297–319.

706 [40] T. C. Gasser, R. W. Ogden, G. A. Holzapfel, Hyperelastic modeling of arterial layers with distributed collagen fiber
707 orientations, J. R. Soc. Interface 3 (6) (2006) 15–35.

708 [41] A. Eilaghi, J. G. Flanagan, I. Tertinegg, C. A. Simmons, G. Wayne Brodland, C. R. Ethier, Biaxial mechanical
709 testing of human sclera, J. Biomech. 43 (9) (2010) 1696–1701

710 [42] M. Á. Ariza-Gracia, D. P. Piñero, J. F. Rodriguez-Matas, R. J. Pérez-Cambrodí, B. Calvo, Interaction between
711 diurnal variations of intraocular pressure, pachymetry, and corneal response to an air puff: Preliminary evidence,
712 JCRS Online Case Reports 3 (2015) 12–15.

713 [43] C. C. Chang, C. J. Lin, Libsvm: a library for support vector machines, ACM T. Intel. Syst. Tech. 2 (3) (2011) 27.

714 [44] Y. Sakamoto, M. Ishiguro, G. Kitagawa, Akaike information criterion statistics, D. Reidel Publishing Company,
715 1999.

716 [45] T. Huseynova, G. O. Waring, 4th, C. Roberts, R. R. Krueger, M. Tomita, Corneal biomechanics as a function of
717 intraocular pressure and pachymetry by dynamic infrared signal and scheimpflug imaging analysis in normal eyes,
718 Am. J. Ophthalmol. 157 (4) (2014) 885–893.

719 [46] J. Simo, On a fully three-dimensional finite-strain viscoelastic damage model: formulation and computational
720 aspects, Comput. Methods Appl. Mech. Engrg. 60 (2) (1987) 153–173.

721 [47] Benoit, Aurélie and Latour, Gaël and Marie-Claire, Schanne-Klein and Allain, Jean-Marc. Simultaneous mi-

crostructural and mechanical characterization of human corneas at increasing pressure., J Mech Behav Biomed Mater, 60 (2016) 93–105 DOI: 10.1016/j.jmbbm.2015.12.031

[48] Gusachenko, Ivan and Tran, Viet and Goulam Houssen, Yannick and Allain, Jean-Marc and Schanne-Klein, Marie-Claire, Polarization-resolved second-harmonic generation in tendon upon mechanical stretching., Biophys J, 102:9 (2012) 2220–2229 DOI: 10.1016/j.bpj.2012.03.068

[49] Latour, Gaël and Gusachenko, Ivan and Kowalczuk, Laura and Lamarre, Isabelle and Schanne-Klein, Marie-Claire, In vivo structural imaging of the cornea by polarization-resolved second harmonic microscopy., Biomed Opt Express, 3:1 (2012) 1–15 DOI: 10.1364/BOE.3.000001

[50] Meek, Keith M. and Boote, Craig., The use of X-ray scattering techniques to quantify the orientation and distribution of collagen in the corneal stroma., Prog Retin Eye Res, 28:5 (2009) 369–392 DOI: 10.1016/j.preteyeres.2009.06.005

[51] Winkler, Moritz and Chai, Dongyul and Kriling, Shelsea and Nien, Chyong Jy and Brown, Donald J. and Jester, Bryan and Juhasz, Tibor and Jester, James V., Nonlinear optical macroscopic assessment of 3-D corneal collagen organization and axial biomechanics., Invest Ophthalmol Vis Sci, 52:12 (2011) 8818–8827 DOI: 10.1167/iovs.11-8070

[52] Winkler, Moritz and Shoa, Golroxan and Xie, Yilu and Petsche, Steven J. and Pinsky, Peter M. and Juhasz, Tibor and Brown, Donald J. and Jester, James V., Three-dimensional distribution of transverse collagen fibers in the anterior human corneal stroma., Invest Ophthalmol Vis Sci, 54:12 (2013) 7293–7301 DOI: 10.1167/iovs.13-13150

[53] Winkler, Moritz and Shoa, Golroxan and Tran, Stephanie T. and Xie, Yilu and Thomasy, Sarah and Raghunathan, Vijay K. and Murphy, Christopher and Brown, Donald J. and Jester, James V., A Comparative Study of Vertebrate Corneal Structure: The Evolution of a Refractive Lens., Invest Ophthalmol Vis Sci, 56:4 (2015) 2764–2772 DOI: 10.1167/iovs.15-16584

[54] Simonini I., Pandolfi A., Customized Finite Element Modelling of the Human Cornea., PLoS One, 10:6 (2015) DOI: 10.1371/journal.pone.0130426

[55] Simonini I., Pandolfi A., The influence of intraocular pressure and air jet pressure on corneal contactless tonometry tests., J Mech Behav Biomed Mater, 58 (2016) 75–89 DOI: 10.1016/j.jmbbm.2015.07.030

[56] Simonini I., Angelillo M., Pandolfi A., Theoretical and numerical analysis of the corneal air puff test, Journal of the Mechanics and Physics of Solids, 93 (2016) 118–134 DOI: 10.1016/j.jmps.2016.04.012

[57] Rosenblatt, F. Principles of Neurodynamics: Perceptrons and the Theory of Brain Mechanisms. Spartan Books, Washington DC, 1961

[58] Cortes C., Vapnik V., Support-vector Networks, Machine Learning, 20:3 (1995), 273–297, DOI: 10.1007/BF00994018

[59] Drucker H., Burges C. J. C., Kaufman L., Smola A. J., Alexander J., Vapnik V. N. Support Vector Regression Machines, Advances in Neural Information Processing Systems, 9 (1996), 155–161

[60] Douglas C. M., Design and Analysis of Experiments, John Wiley & Sons, 5ed (2001) ISBN 0-471-31649-0

Vitae

M. A. Ariza–Gracia

[h] 

He received the B.E. + M.Sc.E. degree in Industrial Engineering from the University of Zaragoza (Zaragoza, Spain) in 2013. In 2014, he received his M.Sc. in Biomedical Engineering. He worked in the European Project: System Based on 3D plenoptic Imaging for Dynamic Topographical Corneal Characterization (PopCorn). Currently, he is a Ph. D student in the Aragón Institute of Engineering Research (i3A, Zaragoza, Spain), with his thesis focusing on Computational Corneal Biomechanics.

S. Redondo

[h] 

He received the B.E. + M.Sc.E in Electrical Engineering from the University of Zaragoza (Information and Communication Technologies specialization) and worked in the private sector on traditional and Vo-IP telephony networks and their integration with business logic applications. In 2015 received the M.Sc. in Biomedical Engineering from the University of Zaragoza focusing on the application of Machine Learning techniques.

[h] 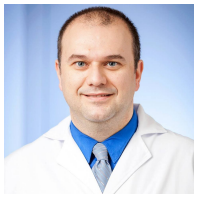

D. P. Piñero

Degree in Optics and Optometry by the University of Alicante (1998) and Degree in Information and Documentation by the Open University of Catalonia (2006). He obtained his PhD Degree in the University of Alicante in 2010 with the doctoral thesis entiled 'Characterization and modeling of the effect of the intrastromal ring segments de in ectatic corneas'. Likewise, he obtained the qualification of University Specialist in Pre- and Post-surgical Optometry by the University of Valladolid in 2001. Currently, he is assistant professor at the Department of Optics, Pharmacology and Anatomy of the University of Alicante, scientific coordinator of the Foundation for the Visual Quality (FUNCAVIS), and head of the Research Unit of OFTALMAR (Vithas Medimar International Hospital, Alicante, Spain).

B. Calvo

[h] 

Became Professor of the Department of Mechanical Engineering of the University of Zaragoza (Spain) in 2010. From 1997 to 2010 she was Associate Professor of Structural Mechanics at the same university. She got the degree of Mechanical Engineering at the University of Zaragoza (Spain) in 1989. She achieved his Ph.D. in Computational Mechanics at the University of Zaragoza in 1994. She is member of the I3A and the CIBER-BBN. Her research is related to Biomechanics in the field of Mechanics of the Soft Tissues, mechanical behaviour of biomaterials and prostheses for clinical applications and experimental methods to characterize biological

tissues.

J. F. Rodríguez

[h] 

He received the B.E. degree in mechanical engineering from Universidad Simón Bolívar, Caracas (Venezuela) in 1993, and the Ph.D. degree in mechanical engineering from the University of Notre Dame (USA) in 1999. He was associated professor at Universidad Simón Bolívar from 2001 to 2004. In 2004 he moved to the Mechanical Engineering Department at Universidad de Zaragoza, Zaragoza (Spain) as a Ramón y Cajal fellow, becoming associate professor in 2011. In 2015 he moved to the Chemistry, Materials and Chemical Engineering Department 'Giulio Natta' at Politecnico di Milano were he is currently associate professor. His research interests concern numerical methods, the biomechanics of sot tissues, vascular biomechanics, and cardiac electrophysiology. He is particularly involved in the material modelling and nonlinear finite element applications, as well as the development of efficient computational tools for cardiac electrophysiology.

Figures

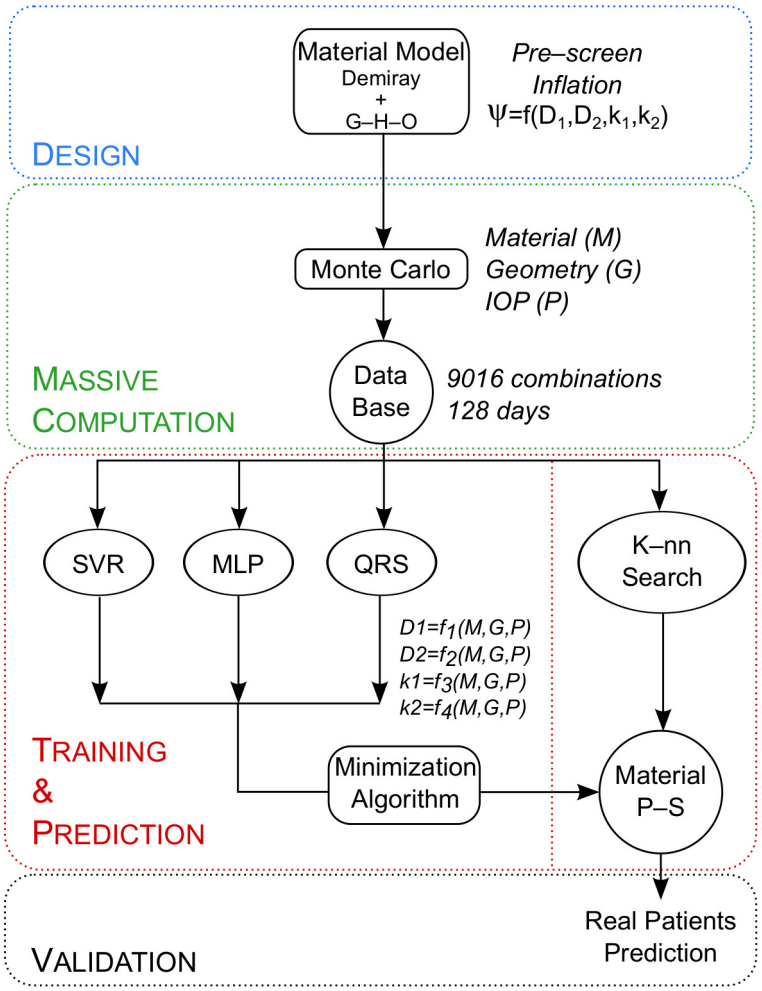

Figure A.9: **Figure 1**

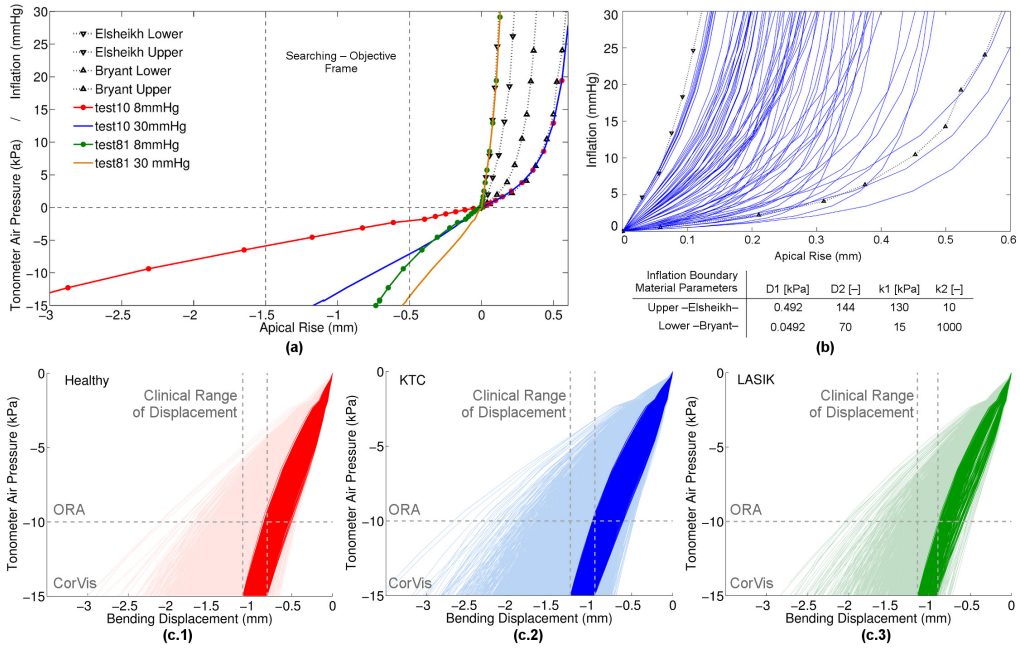

Figure A.10: **Figure 2**

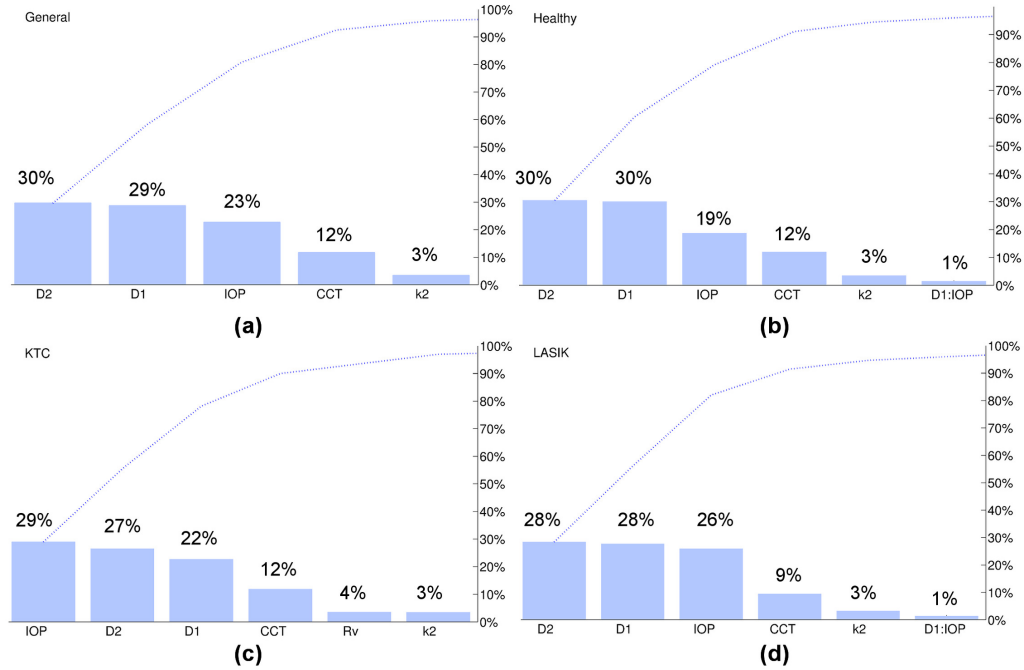

Figure A.11: **Figure 3**

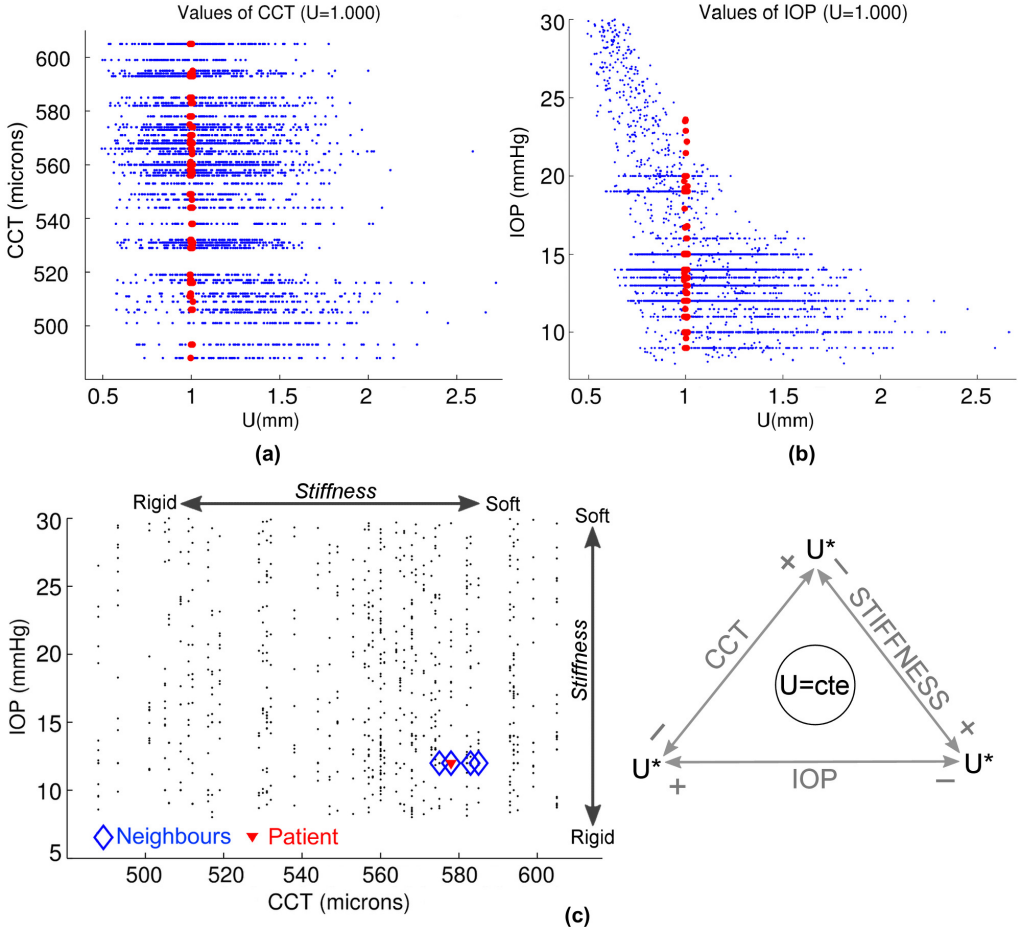

Figure A.12: **Figure 4**

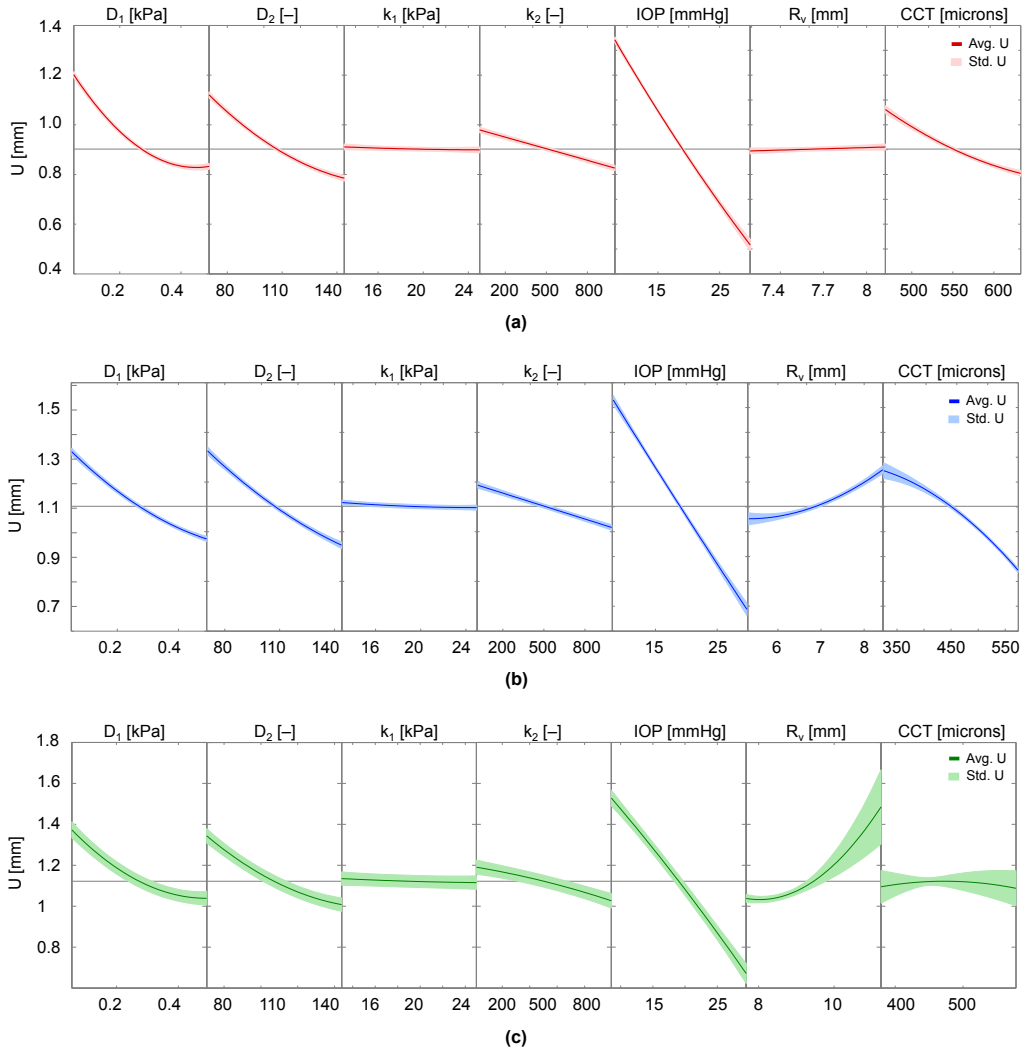

Figure A.13: **Figure A5**

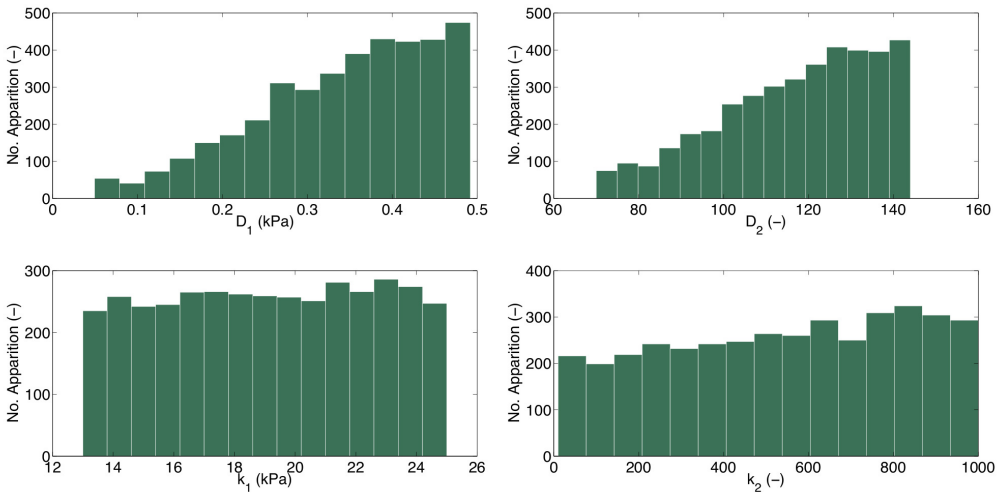

Figure A.14: **Figure A6**

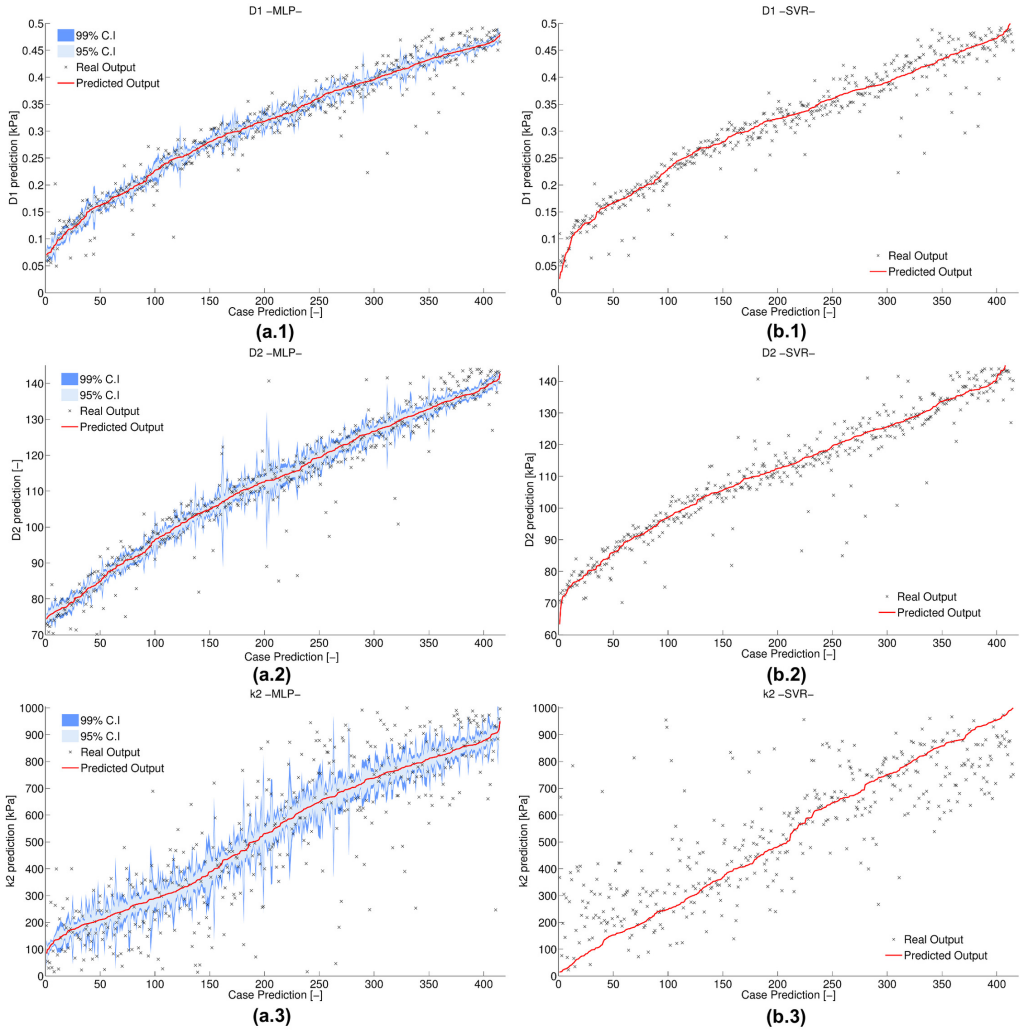

Figure A.15: **Figure A7**

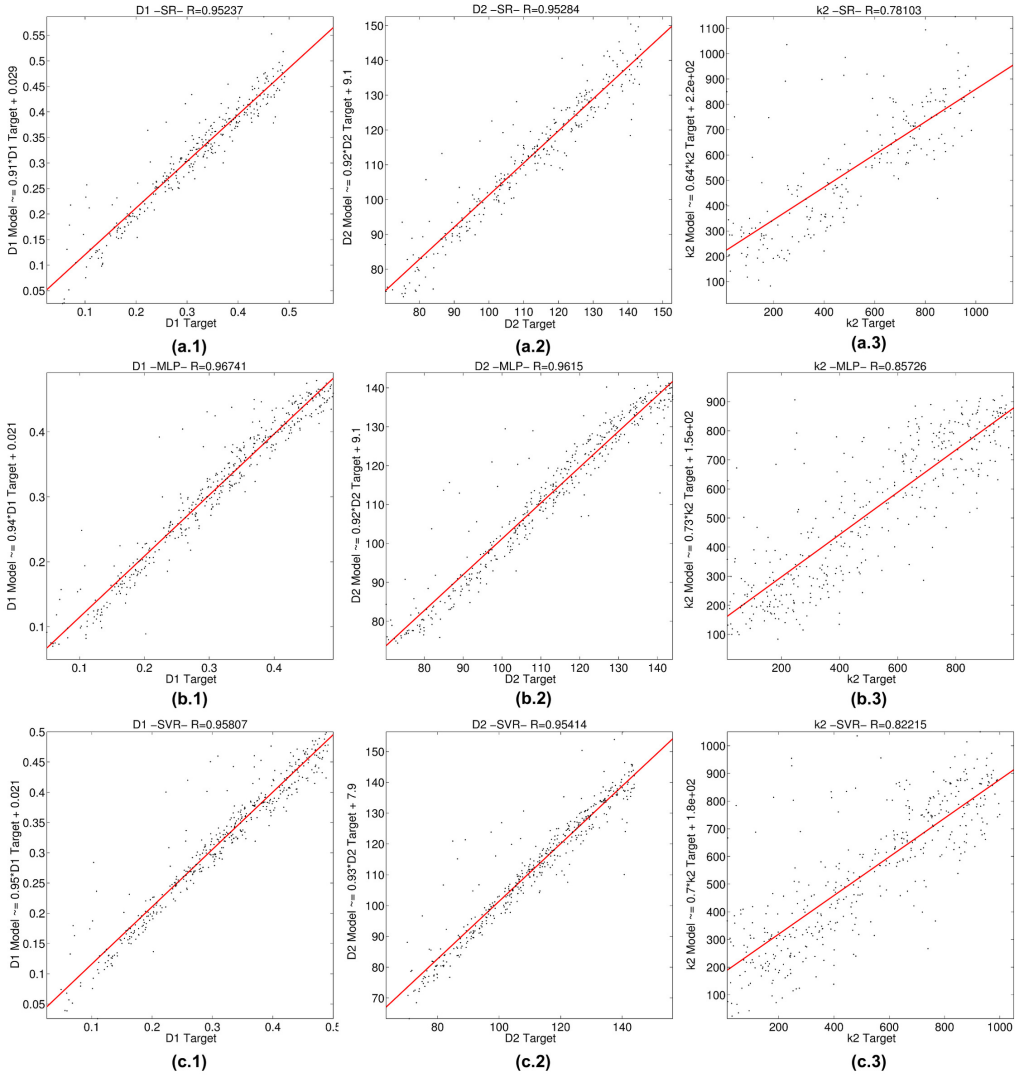

Figure A.16: **Figure A8**